

Multi-task Paired Masking with Alignment Modeling for Medical Vision-Language Pre-training

Ke Zhang, Hanliang Jiang, Jian Zhang, Qingming Huang, *Fellow, IEEE*, Jianping Fan, Jun Yu, *Senior Member, IEEE*, and Weidong Han

Abstract—In recent years, the growing demand for medical imaging diagnosis has brought a significant burden to radiologists. The existing Med-VLP methods provide a solution for automated medical image analysis which learns universal representations from large-scale medical images and reports and benefits downstream tasks without requiring fine-grained annotations. However, the existing methods based on joint image-text reconstruction neglect the importance of cross-modal alignment in conjunction with joint reconstruction, resulting in inadequate cross-modal interaction. In this paper, we propose a unified Med-VLP framework based on Multi-task Paired Masking with Alignment (MPMA) to integrate the cross-modal alignment task into the joint image-text reconstruction framework to achieve more comprehensive cross-modal interaction, while a global and local alignment (GLA) module is designed to assist self-supervised paradigm in obtaining semantic representations with rich domain knowledge. To achieve more comprehensive cross-modal fusion, we also propose a Memory-Augmented Cross-Modal Fusion (MACMF) module to fully integrate visual features to assist in the process of report reconstruction. Experimental results show that our approach outperforms previous methods over all downstream tasks, including uni-modal, cross-modal and multi-modal tasks.

Index Terms—Medical vision-language pre-training, joint image-text reconstruction, cross-modal alignment.

I. INTRODUCTION

Advances in medical imaging technology have improved medical practice, yet the growing number of images has also placed a greater burden on radiologists. Meanwhile, deep learning for automatic medical image analysis requires time-consuming and laborious manual labeling of large-scale medical datasets. To address this issue, existing works use information-rich medical reports to provide supervised signals,

i.e., Medical Vision-Language Pre-training (Med-VLP). Med-VLP aims to learn generic representations from large-scale medical image-text data that can be utilized for various medical visual and textual tasks (e.g., Medical Visual Question Answering, medical image classification and medical report generation), alleviating the problem of insufficient data volume in downstream tasks. Compared to supervised learning, self-supervised Med-VLP does not require manual object-level annotations and learn aligned mapping and semantic representation from the latent space of raw text and images. However, Med-VLP still faces significant challenge since the publicly available dataset for radiology is generally small, with only a few hundred thousand of image-text pairs [1], unlike the natural domain that starts with millions of data (e.g., [2] collected 400 million natural image-text pairs for self-supervised training).

At present, the existing studies of Med-VLP mainly focus on two aspects. One is to improve the pre-training of cross-modal alignment based on ConVIRT [3], and the other is the recently proposed joint image-text reconstruction for self-supervised pre-training, which uses the currently popular MAE method. For the latter method, [4] implements unified multi-modal transformers with normal cross attention while [5] utilizes visual information to assist in report reconstruction with only a simple GAP to perform cross-modal fusion. The joint image-text reconstruction transforms two modalities into a whole, promoting each other. Nonetheless, current studies neglect the importance of cross-modal alignment in conjunction with joint reconstruction, resulting in inadequate cross-modal interaction.

Driven by the above analysis, we propose a unified Med-VLP framework based on Multi-task Paired Masking with Alignment (MPMA) to integrate the cross-modal alignment task into the existing joint image-text reconstruction framework to achieve more comprehensive cross-modal interaction, while utilizing cross-modal alignment task to assist self-supervised paradigm to obtain semantic representations with rich domain knowledge. To the best of our knowledge, there is no complete integration of the two in the medical field currently. We have designed a global and local alignment (GLA) module for cross-modal alignment tasks, and in order to achieve more comprehensive cross-modal fusion, we have proposed a Memory-Augmented Cross-Modal Fusion (MACMF) module to fully integrate visual features to assist in the process of report reconstruction. We performed pre-training on two large-scale medical datasets, i.e., MIMIC-CXR [1] and ROCO [6]. To verify the effectiveness and generalization of our pre-training framework, we construct a medical vision-

This work was supported by the National Natural Science Foundation of China under Grants 62125201, 62020106007, 62176230, 61972361. (Corresponding authors: Jun Yu and Weidong Han.)

K. Zhang and J. Yu are with the Key Laboratory of Complex Systems Modeling and Simulation, School of Computer Science and Technology, Hangzhou Dianzi University, Hangzhou, 310018, China (e-mail: ke.zhang@hdu.edu.cn; yujun@hdu.edu.cn).

H. Jiang is with Regional Medical Center for National Institute of Respiratory Diseases, Sir Run Run Shaw Hospital, College of Medicine, Zhejiang University, Hangzhou, 310016, China (e-mail: aock@zju.edu.cn).

J. Zhang is with School of Information Science and Technology, Hangzhou Normal University, China (e-mail: jeyzhang@outlook.com).

Q. Huang is with the School of Computer Science and Technology, University of Chinese Academy of Sciences, Beijing, 101408, China (e-mail: qmhuang@ucas.ac.cn).

J. Fan is with AI Lab at Lenovo Research, 100094, China (e-mail: jfan1@Lenovo.com).

W. Han is affiliated with the Department of Medical Oncology at Sir Run Run Shaw Hospital, College of Medicine, Zhejiang University in Hangzhou, China. Additionally, he is a professor in the College of Mathematical Medicine at Zhejiang Normal University in Jinhua, China (e-mail: hanwd@zju.edu.cn).

language understanding benchmark that includes uni-modal, cross-modal, and multi-modal tasks, i.e., medical image classification, medical report generation, and medical visual question answering.

Our contribution can be summarized as follows:

- We propose a novel Multi-task Paired Masking with Alignment (MPMA) framework for Med-VLP to integrate joint reconstruction tasks and cross-modal alignment tasks, which includes global and local alignment (GLA) module to achieve more effective cross-modal retrieval capabilities to assist self-supervised paradigm in obtaining more sufficient contextual representation.
- In order to fully integrate visual information during report reconstruction, a novel Memory-Augmented Cross-modal Fusion (MA-CMF) module is proposed to fuse multi-modal information adequately.
- Experimental results show that our approach outperforms previous methods on all downstream tasks over six datasets, including uni-modal, cross-modal, and multi-modal tasks, demonstrating strong model generalization capabilities.

II. RELATED WORKS

A. Medical Vision-Language Pre-training

At present, medical vision-language pre-training can be divided into two categories: report-supervised cross-modal alignment pre-training and reconstruction-based self-supervised pre-training.

The report-supervised cross-modal alignment pre-training was first proposed by ConVIRT [3], which used words and sentences in radiological free-text reports as supervision to guide visual representation learning. Compared to the previous strategy of using ImageNet pre-training weights, [3] proposed bidirectional contrastive learning between two modalities, which was more consistent with the high inter-class similarity characteristics of medical images themselves. However, bidirectional comparisons that only focus on global features overlook the importance of local features. To deal with this problem, [7] proposed to obtain more effective supervision by comparing the local similarity between image sub-regions and words from paired reports on the basis of [3]. Besides, [8] believed that only applying [7] was not enough to mine enough semantic information just at the instance level and region level, disease-level alignment should also be added at a higher semantic level. Thus, a new disease-level alignment paradigm [8] was proposed to enforce the cross-modal cluster assignment consistency. On the basis of [7], BioViL [9] proposed a new language model, i.e., CXR-BERT, for natural language reasoning in radiology to improve textual modeling. In addition, a new dataset MS-CXR had also been released, which included partially aligned image bounding boxes with phrase annotations. Based on [3], REFERS [10] proposed to use multiple image views for each patient to learn joint representations and enhance the original visual information. However, due to the fact that the pre-training dataset MIMIC-CXR [1] itself contains images with one to multiple views, selecting cases with multiple views from MIMIC-CXR will

result in a much smaller dataset when the medical data is already scarce. MedKLIP [11] did not modify the pre-training dataset like [10], nor did it directly perform simple feature extraction on medical reports. Instead, it proposed a triplet extraction module to extract the medical-related information from the reports, using the previously extracted medical information to query from a knowledge base with entity translation.

The reconstruction-based self-supervised pre-training methods were mainly inspired by MAE [12] and the self-supervised pre-text task in BERT [13], which used self-supervised reconstruction of images and reports for representation learning. [4] proposed multi-modal masked autoencoders (M3AE), which learned cross-modal domain knowledge by reconstructing missing pixels and tokens from randomly masked images and texts. However, M3AE only used cross attention for cross-modal interaction and did not fully explore the complementarity between image and report completion. To tackle this problem, MRM [5] proposed to directly integrate the cross-modal visual information processed by GAP during report reconstruction to learn knowledge-enhanced semantic representations. Adequate fusion of visual information plays a crucial role in report reconstruction, but neither [4] nor [5] had fully explored the integration. Therefore, in this paper, we propose a Memory-Augmented cross-modal fusion module to fully integrate visual features to assist in the process of report reconstruction. To the best of our knowledge, existing self-supervised paradigms did not explore applying cross-modal alignment to achieve more comprehensive cross-modal interaction. In this paper, we propose to integrate cross-modal alignment pre-training and self-supervised reconstruction pre-training processes, and apply cross-modal alignment task to assist self-supervised paradigm in obtaining semantic representations with rich domain knowledge.

B. Medical Report Generation

According to the development timeline, medical report generation can be divided into Recurrent Neural Network (RNN) based generative model and Transformer based generative model. With reference to the latest progress in computer vision and machine translation, [14] took the lead in proposing an end-to-end encoder-decoder architecture for image captioning. [15] introduced reward for self-critical based on [14], which better encouraged consistency in training and testing performance. [16] believed that decoder should have different attention strategies for different types of words since gradients of non-visual words can mislead or reduce the effectiveness of visual information. Thus, it proposed an adaptive attention model with a visual sentinel, which determined whether to rely more on the image or visual sentinel at each time step.

With the introduction of the Transformer [17], the original RNN-based decoder was gradually been replaced by the Transformer architecture. Due to the inherent ability of the Transformer to encode and decode long paragraphs, [18] proposed a memory-driven transformer with relational memory to record key information of the generation process. [19] focused on the importance of cross-modal mapping that was previously overlooked, and designed a shared memory to

record the alignment between images and texts facilitating the interaction based on [18]. [20] simulated the working mode of radiologists and integrated report retrieval and medical prior knowledge to generate reports. Unlike previous work that directly generated reports, [21] first predicted disease labels from input images, and then learned multi-granularity visual features by hierarchically aligning visual regions and disease labels. Based on the cross-modal memory in [19], [22] proposed to apply reinforcement learning to avoid overlapping valid dependencies due to the lack of direct cross-modal alignment annotations. [23] focused on the issue of data scarcity, taking the lead in applying semi-supervised learning to report generation tasks and proposing a relation-aware mean teacher framework to capture each potential pathological change. Besides, [24] applied pure transformer to jointly enforce better cross-modal alignment and multi-label classification. [25] was the first to propose a visual language pre-training model and specially designed multiple sub-training tasks for report generation. Our work is different from [25] in that our pre-training framework with extra image reconstruction is generic rather than specifically designed for a particular task, and we validate its effectiveness on more downstream tasks.

C. Medical Visual Question Answering

Medical Visual Question Answering (Med-VQA) has become a popular research field in recent years, thanks to the introduction of related large-scale datasets. The existing methods mainly focus on enhancing multi-modal representation and reasoning, including attention mechanisms, bilinear pooling, meta-learning and data augmentation, etc.

SAN [26] was the first to use stacked attention model for multi-step reasoning to identify image regions associated with the questions while BAN [27] utilized low-rank bilinear pooling to reduce the rank of the weight matrix. However, directly applying the above methods from natural domain to medical domain can lead to overfitting. To tackle this problem, [28] applied unsupervised Denoising Auto Encoder (DAE) and supervised meta-learning to utilize a large amount of unlabeled data and learn meta weights adaptable to VQA problems. [29] focused on question-conditioned reasoning and proposed a conditional reasoning-based framework to decouple open-ended and closed-ended questions. Besides, [30] believed that existing methods did not fully utilize the metadata in the dataset, thus a new multiple meta-model quantifying method was proposed to learn meta-annotation and leverage meaningful features.

Some work focuses on applying data augmentation techniques to improve performance. [31] was the first to use data augmentation techniques, attempting to generate new questions using LSTM [32] and template-based approaches. Different from the former, [33] did not directly make changes to images or questions, but instead generated adversarial examples as new augmented data, which also enhanced the ability of the model to resist adversarial attacks. However, the two stages of feature extraction and cross-modal fusion in existing methods are too independent. To deal with this problem, CMSA-MTPT [34] proposed a multi-task pre-training frame-

work to enhance the compatibility and applicability of the pre-trained features for cross-modal fusion, while also generating corresponding pseudo labels for unlabeled data to expand the dataset. Furthermore, VQAMix [35] proposed a simple yet effective data augmentation method that generated new samples by linearly combining any pair of Q&A samples, while designing a conditional-mixed strategy that utilized language-type prior to force mixed samples to be the same category. Different from the pre-training task specifically designed by [34] for Med-VQA, the pre-training tasks introduced in this paper are more universal, which not only achieve state-of-the-art performance in Med-VQA task but also in medical image classification and medical report generation tasks.

III. METHOD

Fig. 1 shows the overview of our proposed vision-language pre-training framework, which consists of three pre-training tasks: image reconstruction task, report reconstruction task, and Global and local alignment (GLA) task. Specifically, image reconstruction task follows MAE [12] to mask image patches, which reduces the redundancy of visual information by masking patches in a large proportion; The report reconstruction task applies WordPiece [36] as the tokenizer, and we propose a memory-augmented cross-modal fusion module to fuse visual and report features to obtain cross-modal representations. With the assistance of visual information, cross-modal representations are fed into the text decoder for report reconstruction. Compared to BERT [13], we increase the masking ratio of report words to enable better cross-modal fusion and interaction with visual information. GLA task aligns paired images with reports using similarity calculation at global and local scales and assists in image and report reconstruction through cross-modal interaction. We designed symmetrical global and local contrastive losses to better align multi-modal representations, while using masked image modeling loss and masked language modeling loss to assist in the reconstruction process of images and reports respectively. The image reconstruction task shares the same vision encoder with the GLA task, while the report reconstruction task and the GLA task use different text encoders. Our pre-training tasks are elaborated as follows.

A. Image Reconstruction

Following MAE [12], we obtain the image representation by masking a large ratio of the image (i.e., 75%) and then reconstructing it. The motivation is to cover more image regions to reduce the redundancy between image regions. In the image reconstruction branch, we use a pure vision transformer as the image encoder, denoting the input image as $I \in \mathbb{R}^{C \times H \times W}$, where C is the number of channels, H and W are the height and width of the image, respectively. After the reshape operation, the image I is split into multiple patches of the same size as $P \times P$ to obtain $I \in \mathbb{R}^{N_p \times P^2 C}$, where $N_p = \frac{H \times W}{P^2}$ is the number of patches. At this point, the image I can be viewed as N patch sequences of size $P^2 \times C$. Then the patches are linearly projected into patch embeddings and add the corresponding position embedding $E_{pos_1} \in \mathbb{R}^{N_p \times D}$,

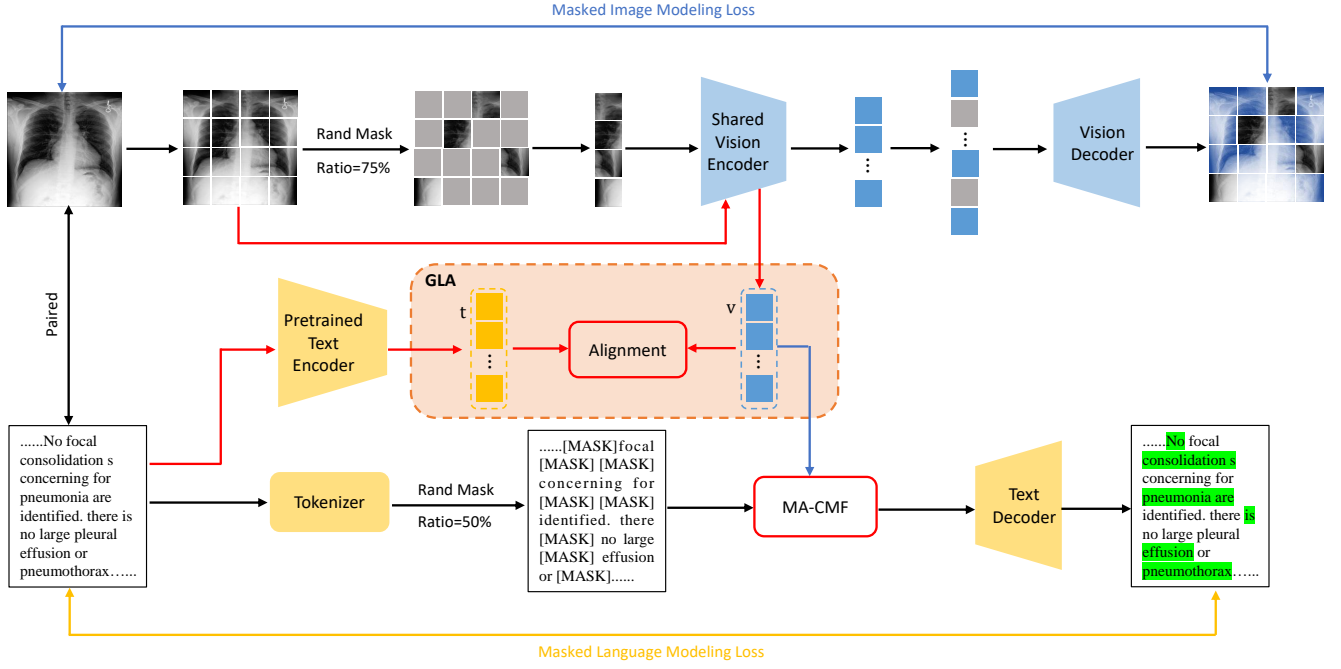


Fig. 1. Overview of our proposed MPMA framework for Med-VLP which consists of three pre-training tasks, namely image reconstruction task, report reconstruction task, and Global and Local Alignment (GLA) task. MA-CMF denotes the Memory-Augmented Cross-Modal Fusion (MA-CMF) module which aggregates the global visual features with report embedding to obtain cross-modal representation for report reconstruction.

which can be formulated as $E_v = IW_{l_1}^T + E_{pos_1}$, where $W_{l_1} \in R^{D \times P^2C}$ is a linear transformation. h patches are selected to be randomly masked using random sampling, the whole image I can be grouped as masked tokens $I_m = \{I_m^1, I_m^2, \dots, I_m^h\}$ (ground truth) and visible unmasked tokens $I_u = \{I_u^1, I_u^2, \dots, I_u^{N_P-h}\}$, then only I_u is fed into the image encoder (denoted as E_I) to obtain its corresponding feature representation $I_U = E_I(I_u) = \{I_U^1, I_U^2, \dots, I_U^{N_P-h}\}$. After image encoding, in order to provide the original position information of the masked tokens, we fill the I_U with position embedding to recover the original N_P size and input it to the image decoder (denoted as D_I) for image reconstruction. The reconstructed image patches is compared with the ground truth patches by the MSE loss function as follows:

$$\mathcal{L}_{MIM}(I_m, I_u) = MSE(I_m^{1:h}, D_I(E_I(I_u^{1:(N_P-h)}))) \quad (1)$$

For the sake of brevity, the process of filling position embedding with $E_I(I_u^{1:(N_P-h)})$ is omitted from the equation.

B. Report Reconstruction

In the report reconstruction branch, reports and images appear in pairs, and we use WordPiece [36] as the tokenizer to convert the report R into tokens as $R = \{r^1, r^2, \dots, r^W\} \in R^{W \times K}$, where the word token $r^w \in R^K$ is represented as one-hot format, K is the dimension of each word piece, and a large ratio of 50% is applied to mask R to obtain the masked part $R_m = \{r_m^1, r_m^2, \dots, r_m^n\}$ (ground truth) and the unmasked part $R_u = \{r_u^1, r_u^2, \dots, r_u^m\}$. Compared to the 15% masking ratio in BERT, we expect a larger percentage of masking (i.e., 50%) to reduce the redundancy of textual information

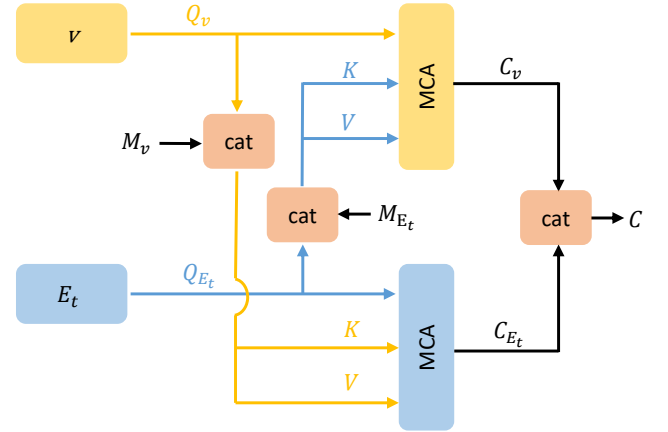


Fig. 2. The proposed Memory-Augmented Cross-Modal Fusion (MA-CMF) module aggregates the global visual features $v = E_I(I)$ with report embedding E_t to obtain cross-modal representation C , where cat denotes the concatenation operation and MCA represents for Multi-head Cross-Attention.

and better fuse cross-modal visual representations for report reconstruction. For the unmasked report token R_u , we add $[MASK]$ at the corresponding position of the mask to keep the same size as the original report R and project R_u into a textual embedding $E_t = R_u W_{l_2}^T + E_{pos_2} \in R^{W \times D}$, where the learnable parameters W_{l_2} are randomly initialized with a fixed dictionary size, and E_{pos_2} is the position embedding for the whole report. Then, in order to use visual information to complement textual information and assist in report reconstruction, a memory-augmented cross-modal fusion module $F(\cdot)$ (as

shown in the Fig. 2) is proposed to aggregate the global visual features $v = E_I(I) \in R^{N_p \times D}$ with report embedding E_t to obtain cross-modal representation C . Among them, in order to more fully integrate cross-modal representations, we do not take a direct concatenation approach, but rather a progressive fusion approach. Firstly, Multi-head Cross-Attention (MCA) is applied to the shallow pre-fusion between visual and textual modality features. MCA is a variant of Multi-head Self Attention (MSA) in different modality input scenarios, which can be formally expressed as:

$$\text{MCA}(Q, K, V) = \underset{i \in \{1, \dots, h\}}{\text{Concat}} \left(\text{Softmax} \left(\frac{QW_i^Q \cdot KW_i^K}{\sqrt{d}} \right) VW_i \right) \quad (2)$$

where $W_i^Q, W_i^K, W_i^V \in R^{d \times \frac{d}{h}}$ are the head projection matrices, h is the number of parallel heads, and $W^M \in R^{d \times d}$ represents the multi-head linear projection. The global visual feature $v = E_I(I) \in R^{N_p \times D}$ with report embedding E_t is fed into MCA to obtain the cross-modal intermediate representation C_v and C_{E_t} . Meanwhile, to better record the modality patterns, we extend the key and value by adding learnable memory matrices, denoted as M_v and M_{E_t} . Thus, the visual and textual pre-fusion processes are formulated as follows:

$$C_v = \text{MCA}(v, [E_t, M_{E_t}], [E_t, M_{E_t}]) \quad (3)$$

$$C_{E_t} = \text{MCA}(E_t, [v, M_v], [v, M_v]) \quad (4)$$

where $[\cdot]$ is the concatenate operation.

The cross-modal global features $C = [C_v, C_{E_t}]$ can be obtained by concatenating the cross-modal intermediate representations C_v and C_{E_t} , which are then fed into the report decoder (simple Transformer architecture) for report reconstruction. Finally, the training is carried out through the loss function of masked language modeling:

$$\mathcal{L}_{\text{MLM}}(R_m, E_t, I_U) = - \sum_{i=1}^n \log P \left(r_m^i \mid E_t^{1:W}, I_U^{1:N_p-h}; \Theta_{E_t}, \Theta_R, \Theta_F \right) \quad (5)$$

where Θ_{E_t}, Θ_R and Θ_F denotes the weight parameters of image encoder, report decoder and memory-augmented cross-modal fusion module, respectively.

C. Global and Local Contrastive Alignment

In order to fully utilize the inter-similarity and intra-similarity between paired images and reports, we propose a global and local alignment module to model the matching of global and local representation, respectively. As shown in Fig. 3, the global and local alignment module shares the same vision encoder with the Image reconstruction task. Different from image reconstruction task, the image is directly sent to the shared vision encoder without random masking after patchifying to obtain the global visual representation $v \in R^{N_p \times D}$ related to the image. The report paired with the image is fed into the pre-trained text encoder (CXRBERT [37]) to obtain global report representations $t \in R^{M \times K}$ corresponding to the report. As shown in Fig. 3, in order to compare global representations in cross-modal space, we first

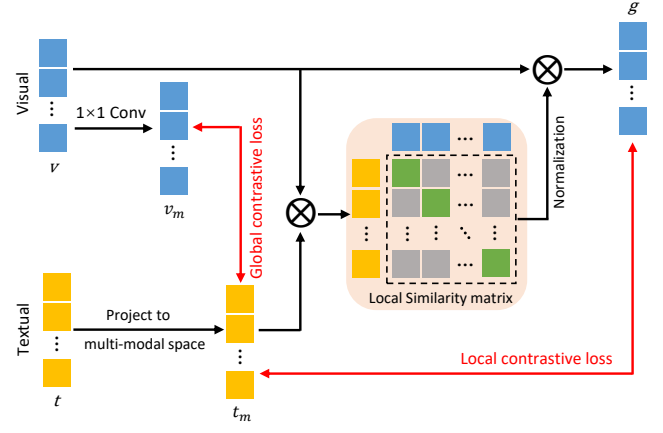


Fig. 3. The calculation process for Global and Local Alignment (GLA) module which models the matching of global and local representation.

use 1×1 convolution to project v into cross-modal space to obtain a cross-modal representation of global visual features $v_m = W_v \cdot v \in R^{M \times D}$, where $W_v \in R^{M \times N_p}$. Then, the global report features are projected into the D -dimensional cross-modal space to obtain $t_m = t \cdot W_t^T \in R^{M \times D}$, where $W_t \in R^{D \times K}$. Denoting $(v_i^m, t_i^m), i \in \{1, 2, \dots, N\}$ as one of paired images and reports among N pairs. It's expected that the global representations between paired v_m and t_m are as close as possible. The symmetric global contrastive loss \mathcal{L}_g is formulated as minimizing the negative log posterior probability to align the inter-similarity between paired images and reports:

$$\mathcal{L}_g = -\frac{1}{N} \sum_{i=1}^N \left(\log \frac{\exp(v_i^m \cdot t_i^m / \tau_1)}{\sum_{j=1}^N \exp(t_i^m \cdot v_j^m / \tau_1)} + \log \frac{\exp(v_i^m \cdot t_i^m / \tau_1)}{\sum_{j=1}^N \exp(v_i^m \cdot t_j^m / \tau_1)} \right) \quad (6)$$

where τ_1 is a scaling factor to control the temperature, and N is the batch size.

For local representation learning, in order to measure the similarity between image regions and report words, we apply dot products to construct a similarity matrix $s = v \cdot t_m^T \in R^{N_p \times M}$. Therefore, the value of s_{ij} measures the degree of correlation between image region v_i and the word t_j . Then, regularization is used to eliminate the influence of similarity scale and obtain the local normalized similarity coefficient matrix α_{ij} :

$$\alpha_{ij} = \frac{\exp s_{ij} / \tau_2}{\sum_{k=1}^{N_p} \exp s_{kj} / \tau_2} \quad (7)$$

where τ_2 is a scaling factor to control the temperature.

Similarity coefficient α_{ij} is utilized to calculate the visual aggregation feature related to the j -th word $g_j = \sum_{i=1}^{N_p} \alpha_{ij} v_i$. It's expected that visual aggregation feature g_j and multi-modal report word features t_j are as close as possible. The

local representation similarity $H(\cdot)$ can be calculated with the following formula:

$$H(X_g, X_t) = \log \sum_{j=1}^M \exp(g_j \cdot t_j) \quad (8)$$

where g_j and t_j correspond to the j -th element in X_g and X_t , respectively.

We extend the calculation of local representation similarity to a batch N and design local contrastive loss \mathcal{L}_1 for learning local representation alignment aligning the intra-similarity between paired images and reports:

$$\mathcal{L}_1 = -\frac{1}{N} \sum_{i=1}^N \left(\log \frac{\exp(\mathbf{H}(\mathbf{X}_{g_i}, \mathbf{X}_{t_i})/\tau_3)}{\sum_{j=1}^N \exp(\mathbf{H}(\mathbf{X}_{g_j}, \mathbf{X}_{t_i})/\tau_3)} + \log \frac{\exp(\mathbf{H}(\mathbf{X}_{g_i}, \mathbf{X}_{t_i})/\tau_3)}{\sum_{j=1}^N \exp(\mathbf{H}(\mathbf{X}_{g_i}, \mathbf{X}_{t_j})/\tau_3)} \right) \quad (9)$$

where τ_3 is a scaling factor to control the temperature, and N is the batch size.

D. Multi-task Training Scheme

We adopt multi-task learning to integrate the loss functions of the pre-training tasks for training. The overall objective function \mathcal{L}_{all} consists of image reconstruction loss \mathcal{L}_{MIM} , report reconstruction loss \mathcal{L}_{MLM} and global and local contrastive losses \mathcal{L}_g and \mathcal{L}_1 :

$$\mathcal{L}_{\text{all}} = \mathcal{L}_{\text{MIM}} + \lambda_{IL} \mathcal{L}_{\text{MLM}} + \lambda_{GLA} (\mathcal{L}_g + \lambda_{gl} \mathcal{L}_1) \quad (10)$$

where the hyper-parameter λ_{IL} balances the loss terms of MIM and MLM tasks, and the hyper-parameter λ_{gl} balances the global and local contrastive loss terms. The hyper-parameter λ_{GLA} determines the weight between GLA task and reconstruction task. Their values will be further discussed in the experiment.

IV. EXPERIMENTS AND RESULTS

To verify the effectiveness of our proposed MPM framework, we finetune and conduct extensive experiments on three tasks, i.e., medical image classification, medical report generation, and medical VQA tasks. The comparisons with the state-of-the-art methods show the effectiveness and generalizability of our proposed MPM framework in multiple medical tasks.

A. Data for Pre-training

We conducted model pre-training on the MIMIC-CXR [1] and ROCO [6] datasets, the descriptions are as follows:

- **MIMIC-CXR**: It is currently one of the largest X-ray datasets containing Chest Radiographs and free-text reports which includes 377110 Chest Radiographs images and 227835 reports from 64588 patients at the Beth Israel Deaconess Medical Center. In the experiment, we use the official splits to partition the dataset into training set with 368960 images and 222758 reports, validation set with 2991 images and 1808 reports, and testing set with 5159 images and 3269 reports. We focus on paired images and reports,

so we only retained the frontal radiographs images with corresponding reports for model pre-training on the training set.

- **ROCO**: It includes image-caption pairs collected from PubMed Central which is an open-access biomedical literature database. It contains over 81000 non-compound medical images with corresponding captions which are randomly split into 65,460/8,183/8,182 for training/validation/testing set. We filter non-radiology samples.

B. Evaluation Tasks & Finetuning Data

1) Medical Image Classification:

- **CheXpert** [38]: A multi-label classification task for Chest X-rays has been defined. We adopt the official setting [38] and selected the most representative 5 lesions for reporting, i.e., atelectasis, cardiomegaly, consolidation, edema, and pleural effusion. Because the official testing set of CheXpert is not open-access, we follow ConVIRT [3] to use the official validation set as the testing set and randomly sampled 5000 images from the training set as the validation set. The training/validation/testing set is divided into 218414/5000/234 images, respectively.
- **RSNA Pneumonia** [39]: A binary classification task has been defined for Chest X-rays, the dataset contains 30k frontal view Chest radiographs labeled as either pneumonia or normal. We use the official splits to divide the training/validation/test set into 25184/1500/3000 images.

2) Medical Report Generation:

- **IU X-Ray** [40]: As the most commonly used benchmark in the medical report generation task, the Indiana University Chest X-ray Collection includes 7470 Chest X-ray images and 3955 corresponding reports. Following previous works [41], [42], we exclude the images without reports and randomly split them by the ratio of 7:2:1 into training, validation and testing set.
- **MIMIC-CXR** [1]: We only use the training set divided in Section IV-A to finetune the model. And the performance is tested on the corresponding testing set.

3) Medical VQA:

- **VQA-RAD** [43]: It contains 3515 question-answer (QA) pairs generated by clinicians, which is split into 3064 QA pairs as training set and 451 QA pairs as test set. There are 11 categories of clinical questions: abnormality, attribute, color, count, modality, organ, plane, positional reasoning, object/condition presence, size, and others. Questions can be divided into closed-ended questions with limited choices and open-ended questions without a limited structure.
- **Path-VQA** [44]: It contains 4,998 pathology images with 32,795 question-answer pairs, which are collected from PEIR digital library and the pathology book. It includes eight types of questions, which are closed-form, ‘what’, ‘where’, ‘when’, ‘how’, ‘why’, ‘whose’, and ‘how much’. The number of questions corresponding to an image varies from 1 to 10.

TABLE I

COMPARATIVE EXPERIMENTS OF MEDICAL IMAGE CLASSIFICATION ON CHEXPert AND RSNA PNEUMONIA DATASET. WE REPORT AUC SCORES UNDER DIFFERENT LABELING RATIOS WHEN FINETUNING ON CHEXPert AND RSNA PNEUMONIA. * DENOTES GLORIA IS IMPLEMENTED BY ViT-B/16.

Method	Input Size	Pre-trained Data	CheXpert			RSNA Pneumonia		
			1%	10%	100%	1%	10%	100%
ConVIRT [3]	224	CheXpert	85.9	86.8	87.3	77.4	80.1	81.3
GLoRIA [7]	224	CheXpert	86.6	87.8	88.1	86.1	88.0	88.6
ConVIRT [3]	224	MIMIC-CXR	87.0	88.1	88.1	88.8	91.5	92.7
MedKLIP [11]	224	MIMIC-CXR	-	-	-	87.3	88.0	89.3
BioViL [9]	480	PubMed+ MIMIC-CXR	-	-	-	88.1	88.4	89.1
GLoRIA* [7]	224	MIMIC-CXR	86.5 \pm 0.8	87.5 \pm 0.6	87.8 \pm 0.5	89.7 \pm 0.8	91.2 \pm 0.5	92.1 \pm 0.3
REFERS [10]	224	MIMIC-CXR	87.2 \pm 0.8	88.1 \pm 0.5	88.2 \pm 0.3	89.4 \pm 0.7	91.6 \pm 0.7	92.7 \pm 0.4
M3AE [4]	224	MIMIC-CXR	86.2 \pm 0.6	87.3 \pm 0.6	87.9 \pm 0.4	89.0 \pm 0.5	90.8 \pm 0.6	92.3 \pm 0.3
MGCA [8]	224	MIMIC-CXR	88.8	89.1	89.7	89.1	89.9	90.8
MRM [5]	224	MIMIC-CXR	88.5 \pm 0.7	88.5 \pm 0.6	88.7 \pm 0.3	91.3 \pm 0.6	92.7 \pm 0.4	93.3 \pm 0.4
Our	224	MIMIC-CXR	89.1 \pm 0.8	89.8 \pm 0.5	90.6 \pm 0.4	91.3 \pm 0.6	93.4 \pm 0.5	94.1 \pm 0.3

C. Experimental Settings

For the implementation, we adopt CLIP-ViT-B [2] as the shared vision encoder and CXR-BERT [9] as the pretrained text encoder. We use center-crop to resize all images to 224 \times 224, and the patch size of ViT is 16 \times 16 with a total of 14 \times 14 patches each image. The masking ratios of images and reports are chosen as 75% and 50%, respectively.

For pretraining, we use AdamW [45] as the optimizer with the learning rate of 2e-4 and weight decay is set to 0.05. MSE loss and cross-entropy loss are used for masking image and language modeling, respectively. The global and local alignment task with two contrasting losses will ramp up from 0 to 1 in the first T epochs to avoid premature forced alignment before the reconstruction task becomes stable. The coefficient λ_{GLA} is determined by a Gaussian warming up function as $\lambda_{GLA}(t) = 1 * e^{-5(1-t/T)^2}$. When λ increases to 1, subsequent training will fix it to 1. λ_{IL} and λ_{gl} are set to 5 and 1 respectively, which will be further investigated in Table VI.

For finetuning, AdamW is used as the optimizer with the learning rate of 5e-6 and 2e-4 for the previous model and the task-specific layers, respectively. For medical image classification (uni-modal) and medical report generation (cross-modal), we adopt pre-trained shared vision encoders as the vision encoders in finetune stage; For medical VQA (multimodal), we adopt shared vision encoder and pre-trained text encoder as the image encoder and question encoder in finetune stage, respectively, while applying our proposed MA-CMF to integrate image and question representation.

For the evaluation metrics, we follow the previous studies to adopt AUC scores for medical image classification, accuracy for medical VQA, and NLG metrics (i.e., BLEU [46], METEOR [47] and ROUGE-L [48]) for medical report generation.

D. Comparison With State-of-the-Art Methods

1) *Medical Image Classification*: We finetune our proposed MPM medical VL pre-training framework using different

ratios of labeled data for medical image classification task on the CheXpert and RSNA Pneumonia datasets. We report classification AUC scores and compare the performance with a series of advanced state-of-the-art pre-training approaches, including ConVIRT [3], GLoRIA [7], MedKLIP [11], BioViL [9], REFERS [10], M3AE [4], MGCA [8], and MRM [5]. Comparison results are quoted from the original papers or [5]. As shown in Table I, MPM achieves significant performance improvement compared to SOTA medical VL pre-training methods under various label ratios on both datasets. It can be seen that when the label ratios are quite small, i.e., 1% and 10%, our MPM considerably surpasses M3AE and REFERS by 2.9%, 2.5% and 1.9%, 1.7% on the CheXpert dataset, and by 2.3%, 2.6% and 1.9%, 1.8% on the RSNA Pneumonia dataset, respectively. This indicates that our pre-training method can still demonstrate strong transferable ability even finetuning with a few data. When finetuning the full ratio of data, our MPM can also surpass M3AE by 1.7% and 2.8% in two datasets, respectively, which fully proves the effectiveness of the pre-training strategies integrating alignment and reconstruction task. Meanwhile, our MPM outperforms advanced MRM on both datasets, which also models the reconstruction tasks, demonstrating the effectiveness of our proposed multi-task modeling scheme.

2) *Medical Report Generation*: We finetune the proposed MPM on medical report generation datasets, i.e., IU X-Ray and MIMIC-CXR, and adopt the widely-used evaluation toolkit [52] to calculate the matching degree between generated reports and ground truth reports, which is reflected by the NLG metrics including BLEU [46], METEOR [47] and ROUGE-L [48]. The current state-of-the-art methods for medical report generation are compared, which includes pre-training methods, i.e., Clinical-BERT [25] and non-pre-training SOTA methods such as R2Gen [18], R2GenCMN [19], PPKED [20], AlignTrans [21], CMM+RL [22], RAMT-U [23], and Multi-Criteria [24]. Comparison results are quoted

TABLE II

COMPARATIVE EXPERIMENTS OF MEDICAL REPORT GENERATION ON IU X-RAY AND MIMIC-CXR DATASET. THE RESULTS ABOUT NLG METRICS ARE REPORTED WHEN FINETUNING ON IU X-RAY AND MIMIC-CXR. B-N, M AND R-L DENOTE BLEU-N, METEOR AND ROUGE-L, RESPECTIVELY.

Method	IU X-Ray						MIMIC-CXR					
	B-1	B-2	B-3	B-4	M	R-L	B-1	B-2	B-3	B-4	M	R-L
Show-Tell [14]	0.346	0.214	0.141	0.095	-	0.320	0.299	0.184	0.121	0.084	-	0.263
Att2in [15]	0.399	0.249	0.172	0.126	-	0.321	0.325	0.203	0.136	0.096	-	0.276
AdaAtt [16]	0.436	0.288	0.203	0.150	-	0.354	0.299	0.185	0.124	0.088	-	0.266
Transformer [17]	0.422	0.264	0.177	0.120	-	0.338	0.314	0.192	0.127	0.090	-	0.265
R2Gen [18]	0.470	0.304	0.219	0.165	0.187	0.371	0.353	0.218	0.145	0.103	0.142	0.277
R2GenCMN [19]	0.475	0.309	0.222	0.170	0.191	0.375	0.353	0.218	0.148	0.106	0.142	0.278
PPKED [20]	0.483	0.315	0.224	0.168	-	0.376	0.360	0.224	0.149	0.106	0.149	0.284
AlignTrans [21]	0.484	0.313	0.225	0.173	0.204	0.379	0.378	0.235	0.156	0.112	0.158	0.283
CMM+RL [22]	0.494	0.321	0.235	0.181	0.201	0.384	0.381	0.232	0.155	0.109	0.151	0.287
RAMT-U [23]	0.482	0.310	0.221	0.165	0.195	0.377	0.362	0.229	0.157	0.113	0.153	0.284
Clinical-BERT [25]	0.495	0.330	0.231	0.170	-	0.376	0.383	0.230	0.151	0.106	0.144	0.275
Multi-Criteria [24]	0.496	0.319	0.241	0.175	-	0.377	0.351	0.223	0.157	0.118	-	0.287
Our	0.518 ± 0.005	0.337 ± 0.005	0.253 ± 0.003	0.179 ± 0.001	0.220 ± 0.003	0.388 ± 0.006	0.392 ± 0.004	0.246 ± 0.004	0.166 ± 0.002	0.122 ± 0.003	0.164 ± 0.003	0.295 ± 0.002

from the original papers. As shown in Table II, our proposed model achieves the best or second-best performance on both datasets. Specifically, compared to the pre-trained Clinical-BERT, our MPM has improved by 5.3% and 3.2% on BLUE-4 and ROUGE-L on the IU dataset, as for the MIMIC dataset, our MPM has improved by 15.1% and 13.9% on BLUE-4 and METEOR, which fully demonstrates the effectiveness of integrating alignment and reconstruction task in the pre-training stage. Compared to the latest non-pre-training method Multi-Criteria, our MPM has significantly improved the performance, especially in BLUE-1, BLUE-4, and ROUGE-L, which have increased by 11.7%, 3.4% and 2.9% on the MIMIC-CXR dataset, respectively. This indicates that multi-task pre-training scheme have indeed helped visual encoder to obtain better feature representation. It is worth noting that our MPM has achieved a greater improvement on BLUE-1 compared to other metrics. The possible reason is that the local alignment in our proposed GLA module makes better alignment between local single words and local single regions so that the single word hit rate gets higher.

3) *Medical VQA*: We finetune our MPM on VQA-RAD and PATH-VQA datasets and compare its performance with the state-of-the-art medical VQA methods, including pre-training approaches, i.e., M3AE [4], MMBERT [51] and MTPT [50], as well as non-pre-training methods such as VQAMix [35], BAN-MEVF+SEADA [33], BAN-MEVF+DAVQA [31] and CMSA-MTPT [34], etc. Among them, VQAMix, BAN-MEVF+SEADA, and BAN-MEVF+DAVQA apply data augmentations to improve performance. Comparison results are quoted from the original papers or [35]. We report mean accuracy on closed-ended and open-ended questions with accuracy overall in Table III, which shows that our proposed MPM achieves the best overall accuracy on both VQA-RAD and PATH-VQA datasets. Specifically, compared to the latest advanced pre-training model M3AE, our MPM showed

an improvement by 2.8%, 2.5% and 3.4% in closed-ended, open-ended questions and overall accuracy on VQA-RAD dataset, and an improvement by 2.2%, 2.8% and 1.4% on PATH-VQA dataset, respectively. This fully demonstrates the effectiveness of integrating alignment and reconstruction tasks in pre-training. Compared to the data augmentation method VQAMix without pre-training, our MPM has significantly surpassed it by 11.6%, 4.6% and 7.2% in closed-ended, open-ended questions and overall accuracy on VQA-RAD dataset, and 3.0%, 3.3% and 1.6% improvements on PATH-VQA dataset, respectively. This indicates that our method not only outperforms the current advanced pre-training methods but also outperforms methods specifically designed for medical VQA task. Overall, the pre-training methods outperform non-pre-training methods in various metrics, which benefit from the learning process of generic feature mapping. Meanwhile, it is worth noting that our MPM has a particularly significant improvement in accuracy compared to VQAMix on open-ended questions. A possible explanation is that our proposed multi-task aggregation paradigm has a better-promoting effect on open-ended questions compared to VQAMix solely based on data augmentation.

E. Reconstruction Analysis

To more clearly demonstrate the reconstruction task in the pre-training, we visualize the masking and reconstruction process of the image and report. Figure 4 shows paired masking and reconstruction examples on MIMIC-CXR dataset. It can be observed that even with high masking ratios, our MPM framework can still restore the vast majority of images and report content. However, a small number of details are lost, e.g., the text reconstruction in the second example, which cannot provide an accurate description of the degree of pleural effusion with incorrectly reconstructing the “moderate sized”

TABLE III
COMPARATIVE EXPERIMENTS OF MEDICAL VQA ON VQA-RAD AND PATH-VQA DATASET. MEAN ACCURACY AND STANDARD DEVIATION ARE REPORTED WHEN FINETUNING ON VQA-RAD AND PATH-VQA. † DENOTES METHODS USING DATA AUGMENTATIONS. * DENOTES OUR IMPLEMENTATION OF M3AE USING ITS OFFICIAL CODE.

Method	VQA-RAD (%)			PATH-VQA (%)		
	Open	Closed	Overall	Open	Closed	Overall
SAN [26]	24.2	57.2	44.0	1.6	59.4	30.5
BAN [27]	27.6	66.5	51.0	2.9	68.2	35.6
SAN-MAML [49]	38.2	69.7	57.1	5.4	75.3	40.5
BAN-MAML [49]	40.1	72.4	60.7	5.9	79.5	42.9
SAN-MEVF [28]	40.7	74.1	60.8	6.0	81.0	43.6
BAN-MEVF [28]	43.9	75.1	62.6	8.1	81.4	44.8
BAN-MEVF+CR [29]	52.4±0.9	79.3±1.1	68.5±1.0	-	-	-
CMSA-MTPT [34]	52.8±1.8	77.8±0.4	67.9±0.8	-	-	-
SAN-MEVF+MMQ [30]	46.3±1.8	73.0±1.4	62.3±1.1	9.6±0.5	83.7±0.4	46.8±0.3
BAN-MEVF+MMQ [30]	52.0±1.1	72.4±0.9	64.3±0.7	11.8±0.6	82.1±0.5	47.1±0.4
BAN-MEVF+DAVQA† [31]	51.2±1.4	76.2±1.4	66.2±1.3	8.5±0.4	83.4±0.2	46.1±0.2
BAN-MEVF+SEADA† [33]	49.6±2.0	72.4±1.5	63.3±1.2	9.1±0.5	81.3±0.3	45.3±0.4
MTPT [50]	61.5	80.9	73.2	-	-	-
MMBERT [51]	63.1	77.9	72.0	-	-	-
SAN-MEVF+VQAMix-C† [35]	53.8±1.9	74.0±2.4	65.9±1.9	12.1±0.5	84.4±0.2	48.4±0.2
BAN-MEVF+VQAMix-C† [35]	56.6±1.3	79.6±1.5	70.4±1.1	13.4±0.6	83.5±0.2	48.6±0.3
M3AE* [4]	65.4±1.4	81.7±1.2	74.2±0.9	14.2±0.7	84.0±0.5	48.8±0.4
Our	68.2±1.1	84.2±1.4	77.6±0.8	16.4±0.5	86.8±0.5	50.2±0.3

TABLE IV
ABLATION STUDY ON THE FOUR KEY COMPONENTS (I.E., IMAGE RECONSTRUCTION LOSS (\mathcal{L}_I), REPORT RECONSTRUCTION LOSS (\mathcal{L}_R), GLOBAL AND LOCAL ALIGNMENT MODULE (GLA) AND MEMORY-AUGMENTED CROSS-MODAL FUSION MODULE (MA-CMF)) ON CHEXPERT (AUC REPORTED), MIMIC-CXR (R-L REPORTED) AND VQA-RAD (OVERALL ACCURACY REPORTED) DATASETS.

\mathcal{L}_I	\mathcal{L}_R	GLA	MA-CMF	CheXpert	MIMIC-CXR	VQA-RAD
✓				84.3	0.260	70.8
✓	✓	✓		87.5	0.279	74.3
✓	✓		✓	88.7	0.286	75.0
✓	✓	✓	✓	90.6	0.295	77.6

to “small sized”. The reason being that the bottom area of the chest cavity in the radiograph is tightly covered, which indirectly proves that the reconstruction of the report requires the assistance of radiograph content and it’s vital to introduce the proposed cross-modal fusion module. For the first example, it is interesting to note that “visualized osseous” was incorrectly identified as “soft tissue”. A possible reason is that “soft tissue” appears in the sentence structure of “... are unremarkable” more frequently than “visualized osseous” and the sternal structures are comprehensively obscured in the image.

TABLE V
ABLATION STUDY ON THE FUSION STRATEGY WHEN INTEGRATING VISUAL AND TEXTUAL REPRESENTATIONS FOR REPORT RECONSTRUCTION ON CHEXPERT DATASET UNDER VARIOUS LABELING RATIOS. AUC SCORES ARE REPORTED.

Fusion Strategy	1%	10%	100%
GAP	85.4	86.0	87.9
GMP	83.2	85.8	88.0
Our CMF	87.5	87.3	89.8
Our MA-CMF	89.1	89.8	90.6

TABLE VI
SENSITIVITY ANALYSIS OF HYPER-PARAMETERS ON CHEXPERT (AUC REPORTED), MIMIC-CXR (R-L REPORTED) AND VQA-RAD (OVERALL ACCURACY REPORTED) DATASETS. λ_{IL} AND λ_{gl} ARE VARIED FOR THE INVESTIGATION. THE DEFAULT VALUES ARE $\lambda_{IL} = 5$ AND $\lambda_{gl} = 1$.

λ_{IL}	λ_{gl}	CheXpert	MIMIC-CXR	VQA-RAD
1	1	89.9	0.288	77.2
5	1	90.6	0.295	77.6
10	1	89.4	0.289	76.2
1	5	88.2	0.273	74.9

F. Qualitative Analysis

As shown in Figure 5, we conduct a qualitative comparison on medical VQA task between M3AE [4] and our proposed







Inputs		[CLS] there [MASK] [MASK] [MASK] . the [MASK] and [MASK] [MASK] are [MASK] [MASK] no focal consolidation [MASK] [MASK] for pneumonia are [MASK] . [MASK] [MASK] no large [MASK] effusion or [MASK] . the visualized osseous structures [MASK] [MASK] .
Reconstruct		[CLS] there is mild cardiomegaly . the hilar and mediastinal contours are normal . no focal consolidation s concerning for pneumonia are identified . there is no large pleural effusion or pneumothorax . the soft tissue structures are unremarkable .
GT		[CLS] there is mild cardiomegaly . the hilar and mediastinal contours are normal . no focal consolidation s concerning for pneumonia are identified . there is no large pleural effusion or pneumothorax . the visualized osseous structures are unremarkable .
Inputs		[CLS] [MASK] [MASK] is status [MASK] [MASK] with sternotomy [MASK] [MASK] to be [MASK] [MASK] . a [MASK] pacemaker [MASK] [MASK] with [MASK] located [MASK] the right [MASK] and right [MASK] [MASK] there is [MASK] [MASK] identified [MASK] [MASK] [MASK] extending [MASK] [MASK] mid svc . a [MASK] sized [MASK] sided pleural [MASK] is [MASK] in addition [MASK] a small left [MASK] [MASK] [MASK] . there [MASK] no focal [MASK] pneumothorax [MASK] [MASK] edema identified [MASK] the heart [MASK] [MASK] at [MASK] upper [MASK] of [MASK] [MASK] mediastinal [MASK] are [MASK] .
Reconstruct		[CLS] the patient is status post cabg with sternotomy wires noted to be well aligned . a biventricular pacemaker is seen with leads located within the right atrium and right ventricle . there is a port-a-cath identified with the tip extending into the mid svc . a small sized right sided pleural effusion is noted in addition to a small left sided pleural effusion . there is no focal consolidation pneumothorax or pulmonary edema identified . the heart size is at the upper limits of normal . mediastinal contours are stable .
GT		[CLS] the patient is status post cabg with sternotomy wires noted to be well aligned . a biventricular pacemaker is seen with leads located within the right atrium and right ventricle . there is a port-a-cath identified with the tip extending into the mid svc . a moderate sized right sided pleural effusion is noted in addition to a small left sided pleural effusion . there is no focal consolidation pneumothorax or pulmonary edema identified . the heart size is at the upper limits of normal . mediastinal contours are stable .

Fig. 4. Paired masking and reconstruction examples on MIMIC-CXR dataset. For each case, we present the masked image with reports (Inputs), our reconstructed pairs (Reconstruct) and the ground truth (GT). Reconstructed and corresponding words are highlighted in green and yellow, respectively.

MPM using Grad-CAM [53] for interpretability. The visualized examples include three modalities, i.e., MRI, CT and X-Ray, on different organs or tissues. The first column is the original images, the second column presents the visualization results of M3AE, the third column displays the visualization results of our MPM, and the last column is the Q&A pairs corresponding to the images.

The first row shows a brain MRI image. Regarding the questions about ventricular abnormalities, M3AE only focuses on the third ventricular hydrocephalus, while our MPM not only focuses on third ventricular hydrocephalus but also on the abnormalities of lateral ventricular hydrocephalus. The second row presents an abdomen CT image, where M3AE locates

the area around the spine, resulting in the wrong answer of calibrated spherosclerosis. In comparison, our MPM correctly answers the question by locating it in ascending colon. The third row shows a chest X-Ray image, and our MPM focuses on the correct position of the lung lobe at the upper left, while M3AE provides a completely opposite position. It can be observed from the visualization results that M3AE indeed only locates the right upper lobe. The chest X-Ray image in the fourth row puts questions on the mass position. In the visualization results, M3AE locates the incorrect area of right lower lateral lung field, while our MPM gives an accurate position through a broader receptive field. The chest X-ray image in the last row still questions the location of abnor-

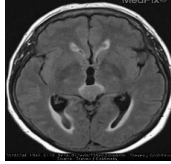
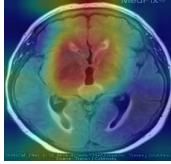
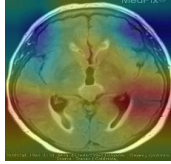

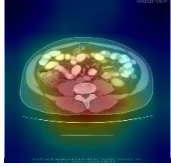
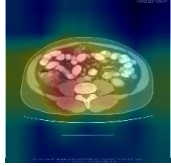









			a Question: What ventricular abnormalities are seen? Answer: Lateral and third ventricular hydrocephalus M3AE: Third ventricular hydrocephalus ✗ Our: Lateral and third ventricular hydrocephalus ✓
			b Question: What is the condition? Answer: Diverticulitis M3AE: Calcified atherosclerosis ✗ Our: Diverticulitis ✓
			c Question: Which lung lobe has the least opacities? Answer: Upper left M3AE: Right upper lobe ✗ Our: Upper left ✓
			d Question: Where is the location of the mass? Answer: Anterior mediastinum M3AE: Right lower lateral lung field ✗ Our: Anterior mediastinum ✓
			e Question: Where is the opacity located? Answer: Right of the midline, superior to the right hilum M3AE: On the right shoulder ✗ Our: Right or left of the midline ✗
Original Image	M3AE	Our	

Fig. 5. Several visualized results on Med-VQA task between the M3AE and our proposed framework. These examples are selected from CT, MRI and X-Ray modalities of VQA-RAD dataset. Red and Green denote the wrong and correct predictions, respectively.

malities. Unfortunately, neither M3AE nor our MPM provided a completely correct answer. Compared to M3AE positioned in the right shoulder, our MPM provided a relatively closer answer. It can be observed that our MPM is more interested in the right and left areas of the midline, where the description of “right of the midline” overlaps with the correct answer. The reason for not accurately locating the region of “superior to the right hilum” may be that the opacity of the image is relatively dense which may be induced by lung inflammation or tumors, and our MPM still has errors in determining this highly fine-grained position. These examples demonstrate that our MPM can more accurately focus on the reasonable regions of the image to answer questions with the help of cross-modal reconstruction and alignment. Still, there is a long way to go to achieve better interpretability.

G. Ablation Study

We conduct an ablation study on the four key components of our proposed framework MPM to evaluate the contribution

of each component, i.e., image reconstruction loss (\mathcal{L}_I), report reconstruction loss (\mathcal{L}_R), global and local alignment module (GLA) and memory-augmented cross-modal fusion module (MA-CMF). As shown in Table IV, experiments are conducted on all three downstream tasks, with AUC scores reported on the CheXpert dataset, R-L Metrics reported on the MIMIC-CXR dataset, and overall accuracy reported on the VQA-RAD dataset. For better evaluation, we remove the other three components only retaining image reconstruction \mathcal{L}_I as a baseline, of which performance drop sharply across all three datasets. When adding report reconstruction \mathcal{L}_R and MA-CMF to the baseline, we can observe a significant improvement in performance. Specifically, performance increased by 5.2%, 10% and 5.9% on classification, report generation and VQA tasks, respectively, which indicates that the pairwise cross-modal fusion after the report reconstruction significantly facilitates the image reconstruction task. It is worth noting that the report generation task on MIMIC-CXR has achieved a larger boost compared to other tasks, indicating that more

adequate cross-modal interaction leads to better downstream task adaptation, especially for the image-to-text modality report generation task. Similarly, with the addition of report construction \mathcal{L}_R and GLA module to baseline, significant performance improvements can still be observed compared to baseline on three tasks with specifically AUC score from 84.3 to 87.5, R-L from 0.260 to 0.279 and overall accuracy from 70.8 to 74.3. It demonstrates that cross-modal alignment is effective for pre-training. Moreover, the performance could be further increased by the integration of GLA and MA-CMF which comes out to be our proposed whole framework. It implies that GLA and MA-CMF can mutually reinforce each other, and adequate cross-modal alignment can better assist in reconstructing the semantic invariance of the task modeling.

We further perform an ablation study to analyze the influence of applying different cross-modal fusion strategies, i.e., global average pooling (GAP), global maximum pooling (GMP), our proposed MA-CMF and its version with the memory part removed (our CMF). As we can see from Table V, our CMF and MA-CMF outperform GAP and GMP by a significant margin, which demonstrates the effectiveness of our proposed cross-modal fusion module. Meanwhile, MA-CMF still shows some performance improvement compared to CMF, indicating that the addition of memory does help better record the modality pattern and assist in accomplishing a more adequate cross-modal fusion.

H. Sensitivity Analysis

We study the sensitivity of different hyperparameter settings for λ_{IL} and λ_{gl} on three datasets with different tasks as shown in Table VI. It can be observed that the performance is not very sensitive when λ_{IL} is greater than or equal to λ_{gl} . However, when fixing the value of λ_{IL} and setting λ_{gl} to 5, the performance on all three datasets shows a significant drop. The reason may be that when the value of λ_{gl} is significantly increased, the weight of the alignment task in multi-task training correspondingly increases, which is harmful to the reconstruction task that has not yet stabilized in the early stage of model training, which also confirms the previous conjecture. As we can see, the optimal performance is achieved when λ_{IL} is equal to 5 and λ_{gl} is equal to 1. Therefore, λ_{IL} and λ_{gl} are set to 5 and 1 in our experiments.

V. CONCLUSION

This work is the first attempt to integrate the cross-modal alignment task into the joint image-text reconstruction framework to achieve more comprehensive cross-modal interaction. We utilize the designed global and local alignment (GLA) module to assist self-supervised paradigm in obtaining semantic representations with rich domain knowledge. In order to achieve more comprehensive fusion, we have proposed a Memory-Augmented Cross-Modal Fusion (MA-CMF) module to fully integrate visual features to assist in the process of report reconstruction. Extensive experiments on six widely-used public benchmark datasets over three downstream tasks demonstrate the superiority of our approach even when using only a few labeled pairs.

REFERENCES

- [1] A. E. Johnson, T. J. Pollard, N. R. Greenbaum, M. P. Lungren, C.-y. Deng, Y. Peng, Z. Lu, R. G. Mark, S. J. Berkowitz, and S. Horng, "Mimic-cxr-jpg, a large publicly available database of labeled chest radiographs," *arXiv preprint arXiv:1901.07042*, 2019.
- [2] A. Radford, J. W. Kim, C. Hallacy, A. Ramesh, G. Goh, S. Agarwal, G. Sastry, A. Askell, P. Mishkin, J. Clark *et al.*, "Learning transferable visual models from natural language supervision," in *International conference on machine learning*. PMLR, 2021, pp. 8748–8763.
- [3] Y. Zhang, H. Jiang, Y. Miura, C. D. Manning, and C. P. Langlotz, "Contrastive learning of medical visual representations from paired images and text," in *Machine Learning for Healthcare Conference*. PMLR, 2022, pp. 2–25.
- [4] Z. Chen, Y. Du, J. Hu, Y. Liu, G. Li, X. Wan, and T.-H. Chang, "Multi-modal masked autoencoders for medical vision-and-language pre-training," in *Medical Image Computing and Computer Assisted Intervention—MICCAI 2022: 25th International Conference, Singapore, September 18–22, 2022, Proceedings, Part V*. Springer, 2022, pp. 679–689.
- [5] H.-Y. Zhou, C. Lian, L. Wang, and Y. Yu, "Advancing radiograph representation learning with masked record modeling," in *The Eleventh International Conference on Learning Representations*, 2023.
- [6] O. Pelka, S. Koitka, J. Rückert, F. Nensa, and C. M. Friedrich, "Radiology objects in context (roco): a multimodal image dataset," in *Intravascular Imaging and Computer Assisted Stenting and Large-Scale Annotation of Biomedical Data and Expert Label Synthesis: 7th Joint International Workshop, CVII-STENT 2018 and Third International Workshop, LABELS 2018, Held in Conjunction with MICCAI 2018, Granada, Spain, September 16, 2018, Proceedings 3*. Springer, 2018, pp. 180–189.
- [7] S.-C. Huang, L. Shen, M. P. Lungren, and S. Yeung, "Gloria: A multimodal global-local representation learning framework for label-efficient medical image recognition," in *Proceedings of the IEEE/CVF International Conference on Computer Vision*, 2021, pp. 3942–3951.
- [8] F. Wang, Y. Zhou, S. Wang, V. Vardhanabhuti, and L. Yu, "Multi-granularity cross-modal alignment for generalized medical visual representation learning," *arXiv preprint arXiv:2210.06044*, 2022.
- [9] B. Boecking, N. Usuyama, S. Bannur, D. C. Castro, A. Schwaighofer, S. Hyland, M. Wetscherek, T. Naumann, A. Nori, J. Alvarez-Valle *et al.*, "Making the most of text semantics to improve biomedical vision-language processing," in *Computer Vision—ECCV 2022: 17th European Conference, Tel Aviv, Israel, October 23–27, 2022, Proceedings, Part XXXVI*. Springer, 2022, pp. 1–21.
- [10] H.-Y. Zhou, X. Chen, Y. Zhang, R. Luo, L. Wang, and Y. Yu, "Generalized radiograph representation learning via cross-supervision between images and free-text radiology reports," *Nature Machine Intelligence*, vol. 4, no. 1, pp. 32–40, 2022.
- [11] C. Wu, X. Zhang, Y. Zhang, Y. Wang, and W. Xie, "Medklip: Medical knowledge enhanced language-image pre-training," *medRxiv*, pp. 2023–01, 2023.
- [12] K. He, X. Chen, S. Xie, Y. Li, P. Dollár, and R. Girshick, "Masked autoencoders are scalable vision learners," in *Proceedings of the IEEE/CVF Conference on Computer Vision and Pattern Recognition*, 2022, pp. 16 000–16 009.
- [13] J. Devlin, M.-W. Chang, K. Lee, and K. Toutanova, "Bert: Pre-training of deep bidirectional transformers for language understanding," *arXiv preprint arXiv:1810.04805*, 2018.
- [14] O. Vinyals, A. Toshev, S. Bengio, and D. Erhan, "Show and tell: A neural image caption generator," in *Proceedings of the IEEE conference on computer vision and pattern recognition*, 2015, pp. 3156–3164.
- [15] S. J. Rennie, E. Marcheret, Y. Mroueh, J. Ross, and V. Goel, "Self-critical sequence training for image captioning," in *Proceedings of the IEEE conference on computer vision and pattern recognition*, 2017, pp. 7008–7024.
- [16] J. Lu, C. Xiong, D. Parikh, and R. Socher, "Knowing when to look: Adaptive attention via a visual sentinel for image captioning," in *Proceedings of the IEEE conference on computer vision and pattern recognition*, 2017, pp. 375–383.
- [17] A. Vaswani, N. Shazeer, N. Parmar, J. Uszkoreit, L. Jones, A. N. Gomez, Ł. Kaiser, and I. Polosukhin, "Attention is all you need," *Advances in neural information processing systems*, vol. 30, 2017.
- [18] Z. Chen, Y. Song, T.-H. Chang, and X. Wan, "Generating radiology reports via memory-driven transformer," in *Proceedings of the 2020 Conference on Empirical Methods in Natural Language Processing (EMNLP)*, 2020, pp. 1439–1449.

- [19] Z. Chen, Y. Shen, Y. Song, and X. Wan, "Cross-modal memory networks for radiology report generation," in *Proceedings of the 59th Annual Meeting of the Association for Computational Linguistics and the 11th International Joint Conference on Natural Language Processing (Volume 1: Long Papers)*, 2021, pp. 5904–5914.
- [20] F. Liu, X. Wu, S. Ge, W. Fan, and Y. Zou, "Exploring and distilling posterior and prior knowledge for radiology report generation," in *Proceedings of the IEEE/CVF Conference on Computer Vision and Pattern Recognition*, 2021, pp. 13 753–13 762.
- [21] D. You, F. Liu, S. Ge, X. Xie, J. Zhang, and X. Wu, "Aligntransformer: Hierarchical alignment of visual regions and disease tags for medical report generation," in *Medical Image Computing and Computer Assisted Intervention–MICCAI 2021: 24th International Conference, Strasbourg, France, September 27–October 1, 2021, Proceedings, Part III 24*. Springer, 2021, pp. 72–82.
- [22] H. Qin and Y. Song, "Reinforced cross-modal alignment for radiology report generation," in *Findings of the Association for Computational Linguistics: ACL 2022*, 2022, pp. 448–458.
- [23] K. Zhang, H. Jiang, J. Zhang, Q. Huang, J. Fan, J. Yu, and W. Han, "Semi-supervised medical report generation via graph-guided hybrid feature consistency," *IEEE Transactions on Multimedia*, 2023.
- [24] Z. Wang, H. Han, L. Wang, X. Li, and L. Zhou, "Automated radiographic report generation purely on transformer: A multicriteria supervised approach," *IEEE Transactions on Medical Imaging*, vol. 41, no. 10, pp. 2803–2813, 2022.
- [25] B. Yan and M. Pei, "Clinical-bert: Vision-language pre-training for radiograph diagnosis and reports generation," in *Proceedings of the AAAI Conference on Artificial Intelligence*, vol. 36, no. 3, 2022, pp. 2982–2990.
- [26] Z. Yang, X. He, J. Gao, L. Deng, and A. Smola, "Stacked attention networks for image question answering," in *Proceedings of the IEEE conference on computer vision and pattern recognition*, 2016, pp. 21–29.
- [27] J.-H. Kim, J. Jun, and B.-T. Zhang, "Bilinear attention networks," *Advances in neural information processing systems*, vol. 31, 2018.
- [28] B. D. Nguyen, T.-T. Do, B. X. Nguyen, T. Do, E. Tjiputra, and Q. D. Tran, "Overcoming data limitation in medical visual question answering," in *Medical Image Computing and Computer Assisted Intervention–MICCAI 2019: 22nd International Conference, Shenzhen, China, October 13–17, 2019, Proceedings, Part IV 22*. Springer, 2019, pp. 522–530.
- [29] L.-M. Zhan, B. Liu, L. Fan, J. Chen, and X.-M. Wu, "Medical visual question answering via conditional reasoning," in *Proceedings of the 28th ACM International Conference on Multimedia*, 2020, pp. 2345–2354.
- [30] T. Do, B. X. Nguyen, E. Tjiputra, M. Tran, Q. D. Tran, and A. Nguyen, "Multiple meta-model quantifying for medical visual question answering," in *Medical Image Computing and Computer Assisted Intervention–MICCAI 2021: 24th International Conference, Strasbourg, France, September 27–October 1, 2021, Proceedings, Part V 24*. Springer, 2021, pp. 64–74.
- [31] K. Kafle, M. Yousefhussein, and C. Kanan, "Data augmentation for visual question answering," in *Proceedings of the 10th International Conference on Natural Language Generation*, 2017, pp. 198–202.
- [32] S. Hochreiter and J. Schmidhuber, "Long short-term memory," *Neural computation*, vol. 9, no. 8, pp. 1735–1780, 1997.
- [33] R. Tang, C. Ma, W. E. Zhang, Q. Wu, and X. Yang, "Semantic equivalent adversarial data augmentation for visual question answering," in *Computer Vision–ECCV 2020: 16th European Conference, Glasgow, UK, August 23–28, 2020, Proceedings, Part XIX 16*. Springer, 2020, pp. 437–453.
- [34] H. Gong, G. Chen, S. Liu, Y. Yu, and G. Li, "Cross-modal self-attention with multi-task pre-training for medical visual question answering," in *Proceedings of the 2021 international conference on multimedia retrieval*, 2021, pp. 456–460.
- [35] H. Gong, G. Chen, M. Mao, Z. Li, and G. Li, "Vqamix: Conditional triplet mixup for medical visual question answering," *IEEE Transactions on Medical Imaging*, vol. 41, no. 11, pp. 3332–3343, 2022.
- [36] Y. Wu, M. Schuster, Z. Chen, Q. V. Le, M. Norouzi, W. Macherey, M. Krikun, Y. Cao, Q. Gao, K. Macherey *et al.*, "Google's neural machine translation system: Bridging the gap between human and machine translation," *arXiv preprint arXiv:1609.08144*, 2016.
- [37] B. Boecking, N. Usuyama, S. Bannur, D. C. Castro, A. Schwaighofer, S. Hyland, M. Wetscherek, T. Naumann, A. Nori, J. Alvarez-Valle *et al.*, "Making the most of text semantics to improve biomedical vision-language processing," in *Computer Vision–ECCV 2022: 17th European Conference, Tel Aviv, Israel, October 23–27, 2022, Proceedings, Part XXXVI*. Springer, 2022, pp. 1–21.
- [38] J. Irvin, P. Rajpurkar, M. Ko, Y. Yu, S. Ciurea-Ilcus, C. Chute, H. Marklund, B. Haghighi, R. Ball, K. Shpanskaya *et al.*, "Chexpert: A large chest radiograph dataset with uncertainty labels and expert comparison," in *Proceedings of the AAAI conference on artificial intelligence*, vol. 33, no. 01, 2019, pp. 590–597.
- [39] G. Shih, C. C. Wu, S. S. Halabi, M. D. Kohli, L. M. Prevedello, T. S. Cook, A. Sharma, J. K. Amorosa, V. Arteaga, M. Galperin-Aizenberg *et al.*, "Augmenting the national institutes of health chest radiograph dataset with expert annotations of possible pneumonia," *Radiology: Artificial Intelligence*, vol. 1, no. 1, p. e180041, 2019.
- [40] D. Demner-Fushman, M. D. Kohli, M. B. Rosenman, S. E. Shooshan, L. Rodriguez, S. Antani, G. R. Thoma, and C. J. McDonald, "Preparing a collection of radiology examinations for distribution and retrieval," *Journal of the American Medical Informatics Association*, vol. 23, no. 2, pp. 304–310, 2016.
- [41] Y. Li, X. Liang, Z. Hu, and E. P. Xing, "Hybrid retrieval-generation reinforced agent for medical image report generation," *Advances in neural information processing systems*, vol. 31, 2018.
- [42] C. Y. Li, X. Liang, Z. Hu, and E. P. Xing, "Knowledge-driven encode, retrieve, paraphrase for medical image report generation," in *Proceedings of the AAAI Conference on Artificial Intelligence*, vol. 33, no. 01, 2019, pp. 6666–6673.
- [43] J. J. Lau, S. Gayen, A. Ben Abacha, and D. Demner-Fushman, "A dataset of clinically generated visual questions and answers about radiology images," *Scientific data*, vol. 5, no. 1, pp. 1–10, 2018.
- [44] X. He, "Towards visual question answering on pathology images," in *Proceedings of the 59th Annual Meeting of the Association for Computational Linguistics and the 11th International Joint Conference on Natural Language Processing*, vol. 2, 2021.
- [45] I. Loshchilov and F. Hutter, "Decoupled weight decay regularization," *arXiv preprint arXiv:1711.05101*, 2017.
- [46] K. Papineni, S. Roukos, T. Ward, and W.-J. Zhu, "Bleu: a method for automatic evaluation of machine translation," in *Proceedings of the 40th annual meeting of the Association for Computational Linguistics*, 2002, pp. 311–318.
- [47] S. Banerjee and A. Lavie, "Meteor: An automatic metric for mt evaluation with improved correlation with human judgments," in *Proceedings of the acl workshop on intrinsic and extrinsic evaluation measures for machine translation and/or summarization*, 2005, pp. 65–72.
- [48] C.-Y. Lin, "Rouge: A package for automatic evaluation of summaries," in *Text summarization branches out*, 2004, pp. 74–81.
- [49] C. Finn, P. Abbeel, and S. Levine, "Model-agnostic meta-learning for fast adaptation of deep networks," in *International conference on machine learning*. PMLR, 2017, pp. 1126–1135.
- [50] H. Gong, G. Chen, S. Liu, Y. Yu, and G. Li, "Cross-modal self-attention with multi-task pre-training for medical visual question answering," in *Proceedings of the 2021 international conference on multimedia retrieval*, 2021, pp. 456–460.
- [51] Y. Khare, V. Bagal, M. Mathew, A. Devi, U. D. Priyakumar, and C. Jawahar, "Mmbert: Multimodal bert pretraining for improved medical vqa," in *2021 IEEE 18th International Symposium on Biomedical Imaging (ISBI)*. IEEE, 2021, pp. 1033–1036.
- [52] X. Chen, H. Fang, T.-Y. Lin, R. Vedantam, S. Gupta, P. Dollár, and C. L. Zitnick, "Microsoft coco captions: Data collection and evaluation server," *arXiv preprint arXiv:1504.00325*, 2015.
- [53] R. R. Selvaraju, M. Cogswell, A. Das, R. Vedantam, D. Parikh, and D. Batra, "Grad-cam: Visual explanations from deep networks via gradient-based localization," in *Proceedings of the IEEE international conference on computer vision*, 2017, pp. 618–626.